



HAL
open science

Opti-Morph, a new platform for sandy beach dynamics by constrained wave energy minimization

Megan Cook, Frédéric Bouchette, Bijan Mohammadi, Samuel Meulé, Nicolas
Fraysse

► **To cite this version:**

Megan Cook, Frédéric Bouchette, Bijan Mohammadi, Samuel Meulé, Nicolas Fraysse. Opti-Morph, a new platform for sandy beach dynamics by constrained wave energy minimization. 2021. hal-03272051v2

HAL Id: hal-03272051

<https://hal.science/hal-03272051v2>

Preprint submitted on 1 Aug 2021 (v2), last revised 13 Mar 2023 (v4)

HAL is a multi-disciplinary open access archive for the deposit and dissemination of scientific research documents, whether they are published or not. The documents may come from teaching and research institutions in France or abroad, or from public or private research centers.

L'archive ouverte pluridisciplinaire **HAL**, est destinée au dépôt et à la diffusion de documents scientifiques de niveau recherche, publiés ou non, émanant des établissements d'enseignement et de recherche français ou étrangers, des laboratoires publics ou privés.

Opti-Morph, a new platform for sandy beach dynamics by constrained wave energy minimization

Megan Cook^{1,3,5}, Frédéric Bouchette^{1,3}, Bijan Mohammadi^{2,3}, Samuel
Meulé^{3,4}, Nicolas Fraysse⁵

¹GEOSCIENCES-M, Univ Montpellier, CNRS, Montpellier, France

²IMAG, Univ Montpellier, CNRS, Montpellier, France

³GLADYS, Univ Montpellier, CNRS, Le Grau du Roi, France

⁴CEREGE, MHN, Aix-en-Provence, France

⁵BRL Ingénierie, Nîmes, France

Key Points:

- A new coastal dynamics morphodynamic model is introduced also accounting for the evolution of the shoreline
- The model automatically adapts to either basin or open sea settings and only requires two hyper-parameters
- Opti-Morph is compared to wave-flume experimental data and XBeach numerical simulations

Corresponding author: Megan Cook, megan.cook@umontpellier.fr

Abstract

This paper focuses on a new approach to describe coastal morphodynamics, based on optimization theory, and more specifically on the assumption that a sandy seabed evolves in order to minimize a wave-related function, the choice of which depends on what is considered the driving force behind the coastal morphodynamic processes considered. The numerical model derived from this theory uses a gradient descent method and allows us to account for physical constraints such as sand conservation in basin experiments. Hence, the model automatically adapts to either basin or open sea settings and only involves two hyper-parameters: sand abrasion and the critical angle of repose. The model behavior is illustrated on a flume configuration. Comparison of the resulting seabed with experimental data as well as the results of the widely distributed coastal morphodynamic software XBeach demonstrate the potential of a model by wave energy minimization.

1 Introduction

Optimization theory is the study of the evolution of a system while searching systematically for the minimum of a function derived from physical properties of the system. In this paper, we have applied this approach to coastal dynamics, with our primary objective to simulate the interactions between the waves and seabed. Continuing the work of (Bouharguane et al., 2010; Mohammadi & Bouharguane, 2011; Bouharguane & Mohammadi, 2012; Mohammadi & Bouchette, 2014) and using mathematical optimization theory, we have designed a model that describes the evolution of the seabed while taking into account the coupling between morphodynamic and hydrodynamic processes. This study focuses on a theoretical and numerical approach to the modeling of this coupling, based on the assumption that the seabed adapts to minimize a certain wave-related function. The choice of this function determines the driving force behind the morphological evolution of the seabed. This optimization problem is subjected to a certain number of constraints, allowing for a more accurate description of the morphodynamic evolution.

This study is accompanied by the development of a numerical hydro-morphodynamic model, which has the advantages of being fast, robust, and of low complexity. The model was given the name *Opti-Morph*.

The paper starts with a description of the simple hydrodynamic model used to calculate the driving forces behind the morphodynamic processes. Then, we provide a description of the morphodynamic model (Opti-Morph) based on wave-energy minimization. With the purpose of validating Opti-Morph, we compare the results of the numerical simulation with that of experimental data acquired in a flume experiment. We also compared the model to another nearshore hydro-morphodynamic model, XBeach (D. J. Roelvink et al., 2009), to see how it fares against existing hydro-morphodynamic models. XBeach is considered to be quite a reputable model in the coastal dynamic community (Zimmermann et al., 2012; Bugajny et al., 2013; Williams et al., 2015).

1.1 State of the Art

Numerical models of morphodynamic processes are seen as a valuable tool for understanding and predicting the evolution of the sediment and morphology over time in coastal areas. Different morphodynamic models exist in the literature, ranging from empirical models (de Vriend et al., 1994; Gravens, 1997; Kana et al., 1999; Ruessink & Terwindt, 2000) to process-based models. The latter can be sorted into several categories, such as i) profile evolution models (Larson & Kraus, 1989; Larson et al., 1990; Nairn & Southgate, 1993), which use only cross-shore transport, ii) 2D

66 morphological models (Fleming & Hunt, 1977; Latteux, 1980; Coeffe & Pechon, 1982;
 67 Yamaguchi & Nishioka, 1985; Watanabe et al., 1986; Maruyama & Takagi, 1988; Wang
 68 et al., 1993; Johnson et al., 1995; Nicholson et al., 1997; D. J. Roelvink et al., 2009),
 69 which use depth-averaged wave and current equations to model the sediment transport
 70 while neglecting the vertical variations of wave-derived parameters, as well as iii) 3D
 71 and quasi-3D models (J. A. Roelvink et al., 1994; Lesser et al., 2004; D. J. Roelvink
 72 et al., 1995; Briand & Kamphuis, 1993; Zyserman & Johnson, 2002; Ding et al.,
 73 2006; Dronen & Deigaard, 2007), which determine the sediment evolution using both
 74 horizontal and vertical variations of the wave-derived parameters.

75 The Opti-Morph model described in this paper is based on optimal control. In
 76 the past, the use of optimization theory has primarily been used in the design of coastal
 77 defense structures, whether in the design of ports and offshore breakwaters (Isebe et
 78 al., 2008; Isèbe et al., 2008).

79 Optimal control has already been envisaged for the modeling of shallow water
 80 morphodynamics, based on the assumption that the seabed acts as a flexible structure
 81 and adapts to a certain hydrodynamic quantity (Mohammadi & Bouharguane,
 82 2011; Bouharguane et al., 2010). These pioneering studies were based on somewhat
 83 theoretical developments with no direct relationship with real case studies. In this
 84 work, we continue along with the objective of producing a physically robust numerical
 85 morphodynamic model based on optimal control and validating it using experimental
 86 and numerical data.

87 1.2 Hypotheses

88 Opti-Morph is based on a certain number of assumptions. Since the model is
 89 based on the minimization of a cost function, certain hypotheses must be made re-
 90 garding the choice of this function. This function, which originates from a physical
 91 quantity, must be directly linked to the elevation of the seabed. At present, we set the
 92 quantity to be minimized as the energy of shoaling waves. This implies that the seabed
 93 reacts to the state of the waves by minimizing the energy of shoaling waves. Other
 94 assumptions assess the behavior of seabed and originate from general observations.
 95 Sediment transport is influenced by the orbital velocity of water particles (Soulsby,
 96 1987), which leads to greater sediment mobility in shallower waters. Another natural
 97 observation concerns the slope of the seabed, which cannot be overly steep without an
 98 avalanching process occurring (Reineck & Singh, 1973). Finally, in an experimental
 99 flume configuration, the quantity of sand must remain constant over time, with no
 100 inflow or outflow of sand to alter the sandstock.

101 2 Theoretical Developments

102 2.1 Modeling Framework

103 For the sake of simplicity, we present the principle of morphodynamics by op-
 104 timization in a one-dimensional setting. This enables us to compare the numerical
 105 results based on this theory with experimental flume data. However, no assumptions
 106 were made regarding the dimension of the problem, and as a result, it is straightforward
 107 to extend this theory to a two-dimensional configuration.

108 We consider a coordinate system composed of a horizontal axis x and a vertical
 109 axis z . We denote $\Omega := [0, x_{\max}]$ the domain of the cross-shore profile of the active
 110 coastal zone, where $x = 0$ is a fixed point in deep waters where no significant change
 111 in bottom elevation can occur, and x_{\max} is an arbitrary point at the shore beyond
 112 the shoreline, as shown by Figure 1. The elevation of the seabed is a one-dimensional
 113 positive function, defined by: $\psi : \Omega \times [0, T] \times \Psi$ where $[0, T]$ is the duration of the

114 simulation (s) and Ψ is the set of physical parameters describing the characteristics of
 115 the seabed. In order to model the evolution over time of ψ and given the assumption
 116 that the seabed ψ changes over time in response to the energy of shoaling waves, a
 117 description of the surface waves is needed.

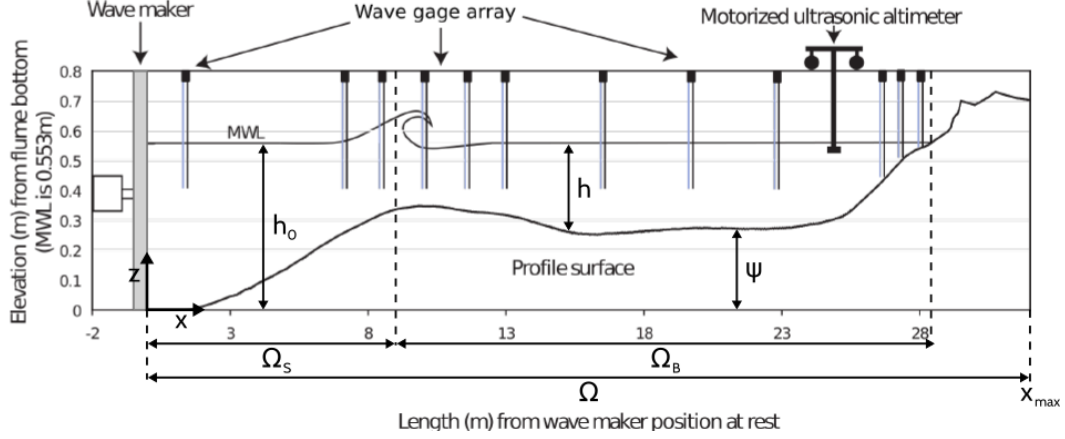


Figure 1: Diagram of a cross-shore profile in the case of an experimental flume.

118 2.2 Hydrodynamic Model

119 The literature on hydrodynamic models is vast (Murray, 2007). However, as our
 120 main focus in this work is on the morphodynamic part of the approach, we present
 121 the procedures with a simple hydrodynamic model based on the linear wave theory
 122 (Dean & Dalrymple, 2004). More sophisticated models may be applied insofar as the
 123 model can be linearized for sensitivity analysis and that the corresponding numerical
 124 implementation has a significantly short run-time. This model has the advantage of
 125 expressing wave height as an explicit function of the seabed, which leads to rapid
 126 calculations of the morphodynamic model.

127 Let h be the depth of the water from a mean water level h_0 (cf. Figure 1).
 128 Ocean waves, here assumed monochromatic, are characterized by phase velocity C ,
 129 group velocity C_g , and wavenumber k , determined by the linear dispersion relation
 130 (1), where σ is the pulsation of the waves and g is the gravitational acceleration.

$$\sigma^2 = gk \tanh(kh) \quad (1)$$

131 We define Ω_S as the time-dependent subset of Ω over which the waves shoal
 132 and Ω_B the subset of Ω over which the waves break, cf. Figure 1. Munk's breaking
 133 criterion (Munk, 1949) enables us to define $\Omega_S(t) = \left\{ x \in \Omega, \frac{H(x,t)}{h(x,t)} < \gamma \right\}$ and
 134 $\Omega_B(t) = \left\{ x \in \Omega, \frac{H(x,t)}{h(x,t)} \geq \gamma \right\}$, where γ is a wave breaking index.

$$H(x, t) = H_0(t) K_S(x, t) \quad (2)$$

135 The height of the waves H over the cross-shore profile is inspired by the shoaling
 136 equation (2), where $H_0(t)$ is the deep water wave height and K_S is a shoaling coefficient,
 137 given by

$$K_S = \left(\frac{1}{2n} \frac{C_0}{C_g} \right)^{\frac{1}{2}} \quad (3)$$

where C_0 is the deep water wave velocity, and:

$$n = \frac{C}{C_g}, \quad C = C_0 \tanh(kh), \quad C_g = \frac{1}{2} C \left(1 + \frac{2kh}{\sinh(kh)} \right). \quad (4)$$

138 Instead of considering that waves depend solely on offshore wave height H_0 , this
 139 model suggests that shoaling waves are decreasingly influenced by seawards waves.
 140 The greater the distance, the less effect it has on the present wave height. As such,
 141 we introduce a weighting function w . Assuming that the maximal distance of local
 142 spatial dependency of a wave is denoted d_w , the weighting function over the maximal
 143 distance d_w is given by $w : [0, d_w] \rightarrow \mathbb{R}^+$ such that $w(0) = 1$, $w(d_w) = 0$ and decreases
 144 exponentially.

Equation (2) for shoaling wave height becomes equation (5), where H_0^w is defined
 by (6).

$$H(x, t) = H_0^w(x, t) K_S(x, t) \quad (5)$$

$$H_0^w(x, t) = \frac{1}{\int_{x-X}^x w(x-y) dy} \int_{x-X}^x w(x-y) H(y) K(y) dy \quad (6)$$

145 Equation (5) applies only to the shoaling, nearshore-dependent waves of Ω_S ,
 146 significant wave height over the cross-shore profile $H : \Omega \rightarrow \mathbb{R}^+$ is defined by (7),
 147 where $\alpha(x) = \frac{x}{d_w}$ over $[0, d_w]$ to allow a smooth transition between offshore and
 148 nearshore-dependent waves.

$$H(x, t) = \begin{cases} [(1 - \alpha(x))H_0(t) + \alpha(x)H_0^w(x, t)] K_S(x, t) & \text{if } x \in \Omega_S \text{ and } x < d_w \\ H_0^w(x, t) K_S(x, t) & \text{if } x \in \Omega_S \text{ and } x \geq d_w \\ \gamma h(x, t) & \text{if } x \in \Omega_B \end{cases} \quad (7)$$

149 2.3 Morphodynamic Model by Wave Energy Minimization

The evolution of the seabed is assumed to be driven by the minimization of a cost
 function J . Recalling the hypotheses made in Section 1.2, the shape of the seabed
 is determined by the minimization of the potential energy of shoaling waves, for all
 $t \in [0, T]$:

$$J(\psi, t) = \frac{1}{16} \int_{\Omega_S} \rho_w g H^2(\psi, x, t) dx \quad [J.m^{-1}] \quad (8)$$

150 where H denotes the height of the waves over the cross-shore profile, ρ_w is water
 151 density ($kg.m^{-3}$), and g is the gravitational acceleration ($m.s^{-2}$). In order to describe
 152 the evolution of the seabed, whose initial state is given by ψ_0 , we assume that the
 153 seabed ψ , in its effort to minimize J , verifies the following dynamics:

$$\begin{cases} \psi_t = \Upsilon \Lambda d \\ \psi(t=0) = \psi_0 \end{cases} \quad (9)$$

154 where ψ_t is the evolution of the seabed over time [$m.s^{-1}$], Υ is the abrasion of sand
 155 [$m.s.kg^{-1}$], Λ is the excitation of the seabed by the water waves, and d is the direction
 156 of the descent, which indicates the manner in which the seabed changes. The approach

157 only involves two hyper-parameters with clear physical interpretation. The first hyper-
 158 parameter Υ takes into account the physical characteristics of the sand and represents
 159 the mobility of the sediment. At the present time, we consider Υ to be a measure
 160 of sand mobility expressed in $m.s.kg^{-1}$. Further explanation of the nature of this
 161 parameter will be given at a later stage of the model's development. The second hyper-
 162 parameter Λ is a local function which represents the influence of the water depth on
 163 the seabed and is defined using an orbital velocity damping function (Soulsby, 1987):

$$\begin{aligned} \varphi : \Omega \times [0, h_0] &\longrightarrow \mathbb{R}^+ \\ (x, z) &\longmapsto \frac{\cosh(k(h - (h_0 - z)))}{\cosh(kh)} \end{aligned} \quad (10)$$

164 In unconstrained circumstances, for instance, if a total sand volume constraint
 165 does not need to be enforced, we set $d = -\nabla_\psi J$, which indicates a direction for local
 166 minimization of J with regards to ψ . The calculation of $\nabla_\psi J$ is described in Ap-
 167 pendix A1. However, constraints are added to the model to incorporate more physics
 168 and deliver more realistic results. Driving forces behind the morphological evolution
 169 of the seabed are described by the minimization of the cost function J . Secondary
 170 processes are expressed by constraints. In the interest of simplicity, we have adopted
 171 two physical constraints though more can be introduced if necessary. The first con-
 172 cerns the slope of the seabed. Depending on the composition of the sediment, the slope
 173 of the seabed is bounded by a grain-dependent threshold M_{slope} (Dean & Dalrymple,
 174 2004). This is conveyed by the following constraint on the local bathymetric slope:

$$\left| \frac{\partial \psi}{\partial x} \right| \leq M_{\text{slope}} \quad (11)$$

175 The dimensionless parameter M_{slope} represents the critical angle of repose of the sed-
 176 iment, and varies between 0.2 and 0.6 (Beakawi Al-Hashemi & Baghabra Al-Amoudi,
 177 2018).

178 A second example concerns the sandstock in the case of an experimental flume.
 179 This constraint states that the quantity of sand in a flume must be constant over time,
 180 as given by (12), contrarily to an open-sea simulation where sand can be transported
 181 between the onshore and the offshore zones (Hattori & Kawamata, 1980; Quick, 1991).

$$\int_{\Omega} \psi(t, x) dx = \int_{\Omega} \psi_0(x) dx \quad \forall t \in [0, T] \quad (12)$$

182 This constraint is necessary for verifying and validating the numerical model with
 183 physical simulations.

184 **3 Numerical Application**

185 In this section, we present the numerical results produced by the Opti-Morph
 186 model. For validation purposes, the resulting seabed is compared to experimental
 187 data acquired during a flume tank experiment. We also conduct a comparative analy-
 188 sis between the physical seabed, the seabed produced by Opti-Morph and the seabed
 189 produced by XBeach, with the aim of assessing how Opti-Morph holds up against exist-
 190 ing hydro-morphodynamic models. A brief description of the experiment is provided,
 191 as well the XBeach model.

192 **3.1 Description of the Experiment**

193 The experimental observations presented here were collected as part of the COPTER
 194 project and a series of laboratory wave-flume experiments were performed in order to

195 investigate the morphodynamic impact of introducing solid geotextile tubes to the
 196 Hatzuk (Israel) seafloor (Bouchette, 2017). We use the data collected without tubes
 197 to describe the natural evolution of the seabed over time.

198 A glass flume measuring 36 m long, 0.55 m wide and 1.3 m deep is equipped with
 199 a wave-maker and gauges measuring the height of the water. Artificial particles are
 200 placed inside the flume representing the mobile sea bottom and an ultrasonic gauge is
 201 used to measure the sedimentary topography.

202 The experimental seabed, described in Figure 1 is subjected to a 30-minute storm
 203 climate, with a significant wave height and period of $H_s = 135\text{ mm}$ and $T_s = 2.5\text{ s}$.
 204 Time and length scale ratio are set to 1/3 and 1/10 respectively to that of the field.

205 3.2 XBeach Model

206 XBeach is an open-source process-based model developed by Deltares, UNESCO-
 207 IHE, and Delft University of Technology to simulate the hydro-morphodynamic pro-
 208 cesses in coastal areas.

209 In brief, XBeach uses four interconnected modules to model near-shore processes
 210 (Daly, 2009). The two hydrodynamic modules consist of the short wave module and
 211 the flow module. The first is based on wave action equations (Holthuijsen et al., 1989),
 212 and incorporates breaking, dissipation (D. J. Roelvink, 1993), and wave current inter-
 213 actions, while the latter is governed by shallow water equations (Andrews & McIntyre,
 214 1978; Walstra et al., 2000). One of the two morphodynamic modules is the sediment
 215 transport module based on the equilibrium sediment concentration equation (Soulsby,
 216 1997) and a depth-averaged advection-diffusion equation (Galappatti & Vreugdenhil,
 217 1985). The other is the morphology module which concerns seabed transformations
 218 such as the evolution of the seabed and avalanching.

219 In order to configure the XBeach model for the experimental flume setting, we
 220 refer to the XBeach user manual (D. J. Roelvink et al., 2010). The domain Ω is defined
 221 over 32 m with a uniform subdivision of 320 cells. The incoming wave boundary
 222 condition is provided using the JONSWAP wave spectrum (Hasselmann et al., 1973),
 223 with a significant wave height of $H_{m0} = 0.015\text{ m}$ and a peak frequency at $f_p = 0.4\text{ s}^{-1}$.
 224 The breaker model uses the Roelvink formulation (D. J. Roelvink, 1993), with a breaker
 225 coefficient of $\gamma = 0.4$, a power $n = 15$, and a wave dissipation coefficient of 0.5.
 226 These parameters were calibrated using the hydrodynamic data produced during the
 227 physical flume experiment. Concerning sediment parameters, the $D50$ coefficient is
 228 set as 0.0006, and the porosity is 2650 kg.m^{-3} . No other parameters such as bed
 229 friction or vegetation were applied. The model is set to run for a period of 1800 s, as
 230 a short-term simulation.

231 3.3 Hydrodynamic Validation

232 This section is devoted to the comparison of the two numerical hydrodynamic
 233 models to the experimental wave data obtained in the experimental flume of Section
 234 3.1. Mean wave height profiles were calculated over the short-term storm simulation,
 235 for both Opti-Morph and XBeach, and compared to the mean wave height of the
 236 experimental model. The latter was calculated using the measures taken by the gauges
 237 of the flume.

238 Figure 2 shows that the hydrodynamic module of both Opti-Morph (red) and
 239 XBeach (blue) are both comparable with respect to the experimental measurements
 240 (green) excluding, as is often the case, the second point at $x = 6\text{ m}$. XBeach demon-
 241 strates a close qualitative fit over the 10-22 m section of the flume, whereas Opti-Morph
 242 excels at the coast (21-27 m), with a near-perfect fit with the experimental data. De-

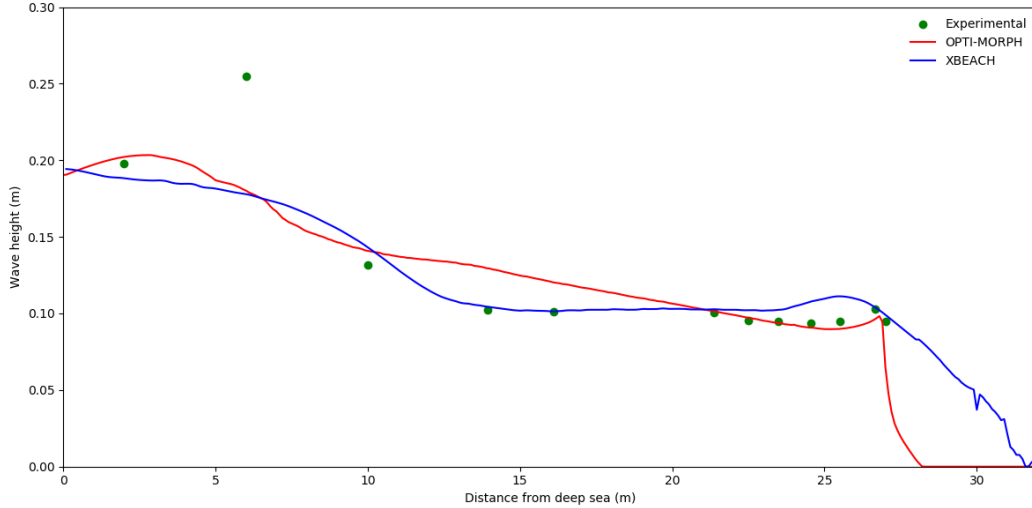


Figure 2: Comparison of mean wave height over a storm simulation. The green points correspond to the mean wave height provided by the gauges of the flume experiment. The mean wave height determined by Opti-Morph (red) and XBeach (blue) also appear. The non-zero wave height beyond the shoreline as presented by XBeach is due to wave set-up, which Opti-Morph doesn't include.

243 spite the simplicity of the hydrodynamic model used by Opti-Morph, the resulting
 244 wave height is of the same order of magnitude over the cross-shore profile than that
 245 measured during the flume experiment, which indicates that the resulting seabeds are
 246 comparable with regard to the forcing energy driving the morphodynamic response.

247 3.4 Numerical Results of the Morphodynamic Simulations

248 The Opti-Morph model was applied to the configuration of the COPTER exper-
 249 iment of Section 3.1, and the resulting beach profile is shown by the red profile, in
 250 Figure 3.A. The main observation is the decrease of 2.5 cm in height of the sandbar,
 251 at $x = 9 m$. We observe a slight decrease of the seabed adjacent to the wave-maker,
 252 and a slight increase at the plateau, situated at 15-25 m. No mobility is observed at
 253 the coast.

254 When comparing the results provided by Opti-Morph (red), with that of XBeach
 255 (blue) and the experimental data (green), as shown on Figure 3.A, we observe that
 256 the red seabed profile provided by the Opti-Morph model shows a general quantitative
 257 agreement when compared to the experimental data, as does the XBeach morphological
 258 module. In fact, both models produce profiles close to the experimental data over the
 259 plateau located at 15-25 m from the wave-maker (Fig. 3.C). At the shore, Opti-Morph
 260 matches the experimental data whereas XBeach shows a vertically difference of up to
 261 3cm at $x = 27 m$ (Fig. 3.D). Discrepancies on the part of both models occur in the area
 262 surrounding the tip of the sandbar, as both Opti-Morph and XBeach fail to predict the
 263 advancing of the sandbar (Fig. 3.B); the experimental data show that the height of
 264 the sandbar remains unchanged with regards to the initial profile. Both sandbars have
 265 a height of 0.375 m, however, the sandbar resulting from the experimental simulation
 266 has advanced towards the coast, an occurrence that neither numerical model was able
 267 to predict.

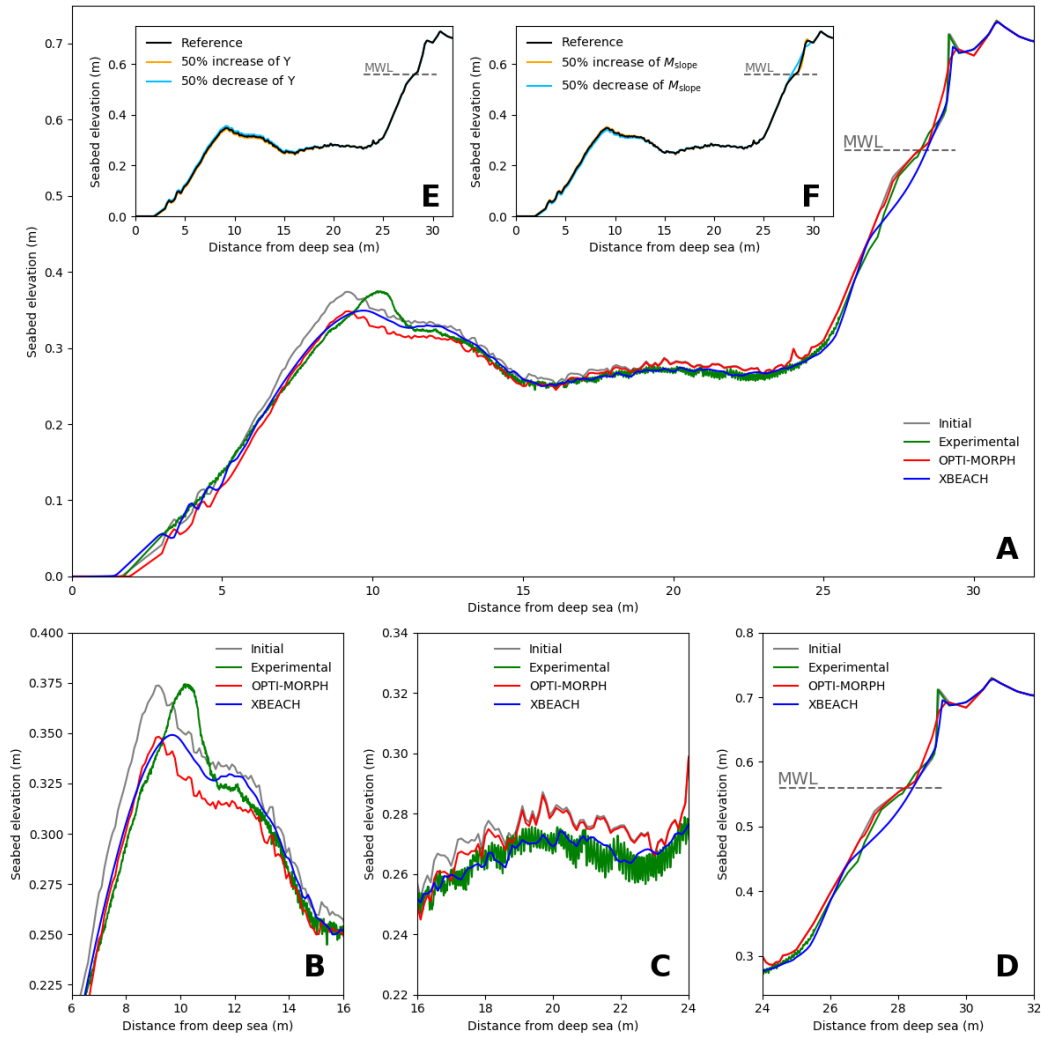


Figure 3: **A.** Results of the numerical simulation calculated over the initial seabed (gray) using the XBeach morphodynamic module (blue) and the Opti-Morph model (red). These are compared with the experimental data acquired during the COPTER project (green). The mean water level is denoted MWL and is set at 0.56 m . **B.** Zoomed in view of the sandbar, located between 6 m and 16 m . **C.** Zoomed in view of the plateau, located between 16 m and 24 m . **D.** Zoomed in view at the shoreline, located between 24 m and 32 m . **E.** Robustness analysis of the mobility parameter Υ . The reference profile is depicted in black. The orange (resp. light blue) profile is the result of a 50% increase (resp. decrease) in mobility, with all other parameters remaining the same. **F.** Robustness analysis of the maximal sand slope parameter M_{slope} . The reference profile is depicted in black. The orange (resp. light blue) profile is the result of a 50% increase (resp. decrease) of M_{slope} , with all other parameters remaining the same.

268
269

As such, this new model based on wave-energy minimization shows potential when compared to XBeach, in the case of short-term simulations.

4 Discussion

4.1 Parameter Robustness Analysis

One of the advantages of the Opti-Morph model is the low number of morphodynamic parameters required. At the present time, Opti-Morph requires two parameters: the mobility parameter Υ and the maximal slope parameter M_{slope} . Here, an assessment on these parameters is conducted. In Figure 3.E, three simulations were performed in identical settings with changes made solely to the mobility parameter. Initially, this parameter Υ has a value of 5×10^{-6} , $m.s.kg^{-1}$. Figure 3.E shows no significant difference despite a 50% increase ($\Upsilon = 7.5 \times 10^{-6} m.s.kg^{-1}$) (orange) or decrease ($\Upsilon = 2.5 \times 10^{-6} m.s.kg^{-1}$) (light blue) of Υ with regard to the baseline seabed profile (black). Similar conclusion can be deduced for the maximal slope parameter M_{slope} , whose reference value here is 0.2. The corresponding parameter of XBeach is *wetslp*, described in the XBeach manual as the critical avalanching slope under water, and is also set to 0.2. In Figure 3.F, we observe little difference between the reference seabed (black), the seabed resulting from a 50% increase ($M_{\text{slope}} = 0.3$) (orange) and the seabed resulting from a 50% decrease ($M_{\text{slope}} = 0.1$) (light blue). The only apparent discrepancy can be found at $x = 28 m$, where the seabed is at its steepest, and therefore the sand slope constraint is more prone to be active. The reduction of the critical angle of repose results naturally in a less steep slope. The robustness of Opti-Morph in relation to both the mobility parameter and the slope parameter, despite a significant increase or decrease of their value, is apparent. Further simulations show that the robustness of these parameters is not specific to this particular flume configuration, but can be observed regardless of the initial configuration.

4.2 Long-term Simulations

This section is devoted to the long-term behavior of Opti-Morph, the main question being, is this numerical model capable of creating an equilibrium state after being subjected to a great number of repeated events. Five forcing scenarios, lasting either 2 or 6 days, were applied to the same initial seabed in the same parametric configuration. The current Opti-Morph code is in Python. Typically, using time-steps of 1 s simulating a day of forcing requires about 1.5 hours on a 2GHz PC computer. Each time iteration gathering the steps presented in this paper requires therefore about 63 ms. An analysis of the resulting seabeds is performed as well as their behavior throughout the simulation. The latter is achieved through a comparative study of four time-series', focusing on: (1), the vertical evolution of seabed elevation at the tip of the sandbar; (2), the vertical evolution of seabed elevation at a point of the plateau; (3), the distance between the wave-maker and the onset of the seabed; and (4), the location of the shoreline position.

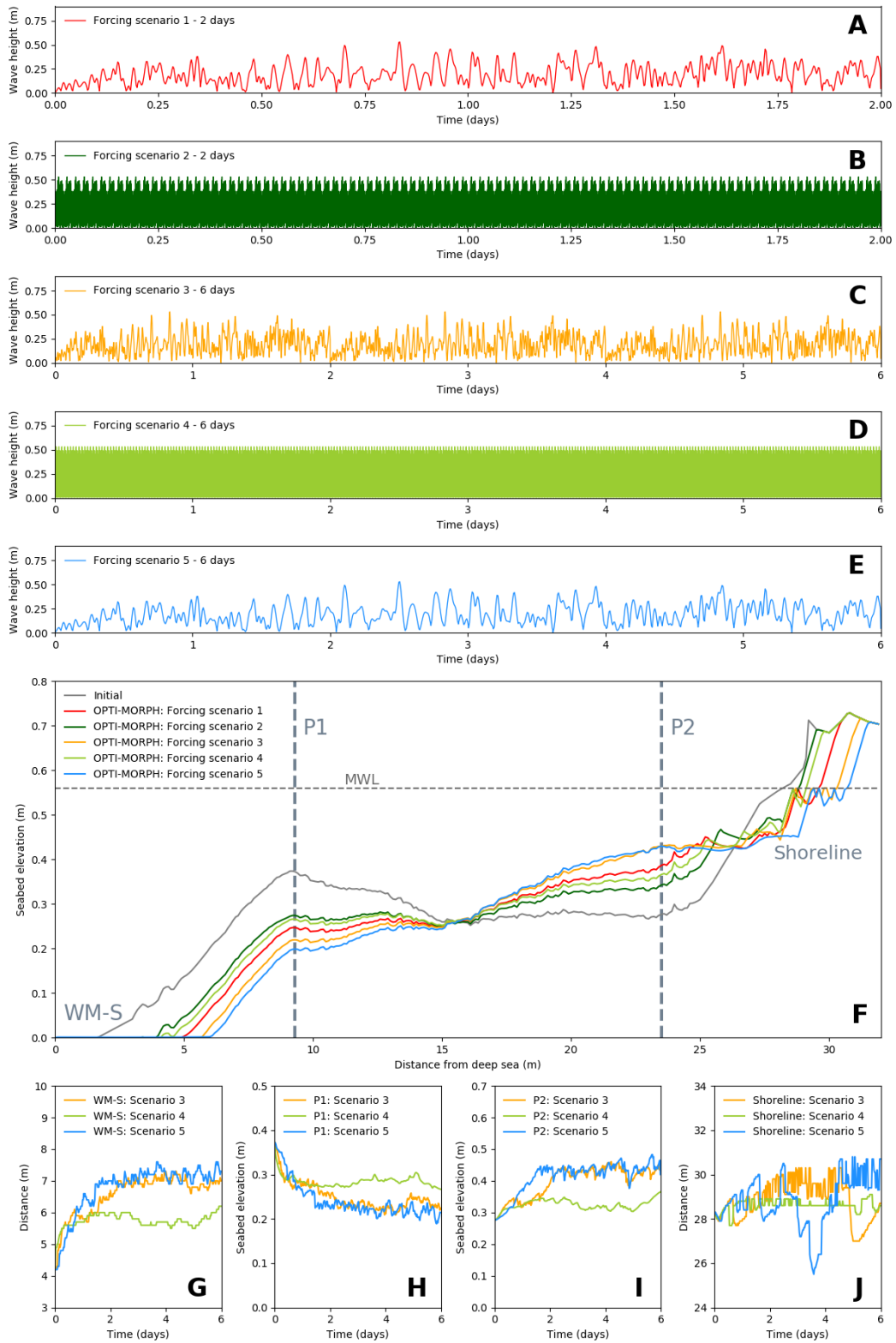


Figure 4: Long-term simulation of Opti-Morph. **A.** Forcing wave height for scenario 1, composed of several long-term events over a 2-day period. **B.** Forcing wave height for scenario 2, composed of numerous short-term events over a 2-day period. **C.** Forcing wave height for scenario 3, composed of several long-term events over a 6-day period. **D.** Forcing wave height for scenario 4, composed of numerous short-term events over a 6-day period. **E.** Forcing wave height for scenario 5, composed of few long-term events over a 6-day period. **F.** Seabeds resulting from the different forcing scenarios produced by Opti-Morph. Two points of interest have been identified: P1 located at $x = 9.3\text{ m}$ and P2 located at $x = 20.1\text{ m}$. **G.** Evolution of the distance, devoid of sediment, between the wave-maker (located at $x = 0\text{ m}$) and the seabed (WM-S), regarding forcing scenarios 3, 4, and 5. **H.** Vertical evolution of seabed elevation at P1, driven by the 6-day forcing scenarios 3, 4, and 5. **I.** Vertical evolution of seabed elevation at P2, driven by the 6-day forcing scenarios 3, 4, and 5. **J.** Evolution of shoreline position, driven by the 6-day forcing scenarios 3, 4, and 5.

307 Applying Opti-Morph over a longer time-series leads to the results of Figure 4.
 308 The two 2-day forcing scenarios are shown in Figures 4.A and 4.B. In both cases,
 309 we observe that the resulting seabeds of Figure 4.F are subjected to the destruction
 310 of the sandbar and have a tendency to evolve progressively towards an equilibrium
 311 beach profile (of Engineers, 2002). Simulations over a 6-day period were conducted
 312 to confirm this tendency. These scenarios are depicted in Figures 4.C, 4.D, and 4.E,
 313 and the resulting seabeds given in Figure 4.F show once again the destruction of the
 314 sandbars, the elevation of the plateau, and erosion at the shoreline. Furthermore,
 315 all three tend towards an equilibrium state. This is confirmed by the four time-series
 316 analysis presented in Figures 4.G, 4.H, 4.I, and 4.J. The vertical elevation of the seabed
 317 at both points P1 and P2 show initial variations over the first 2 days: a decrease in
 318 the case of P1 (cf. Figure 4.H) and an increase in the case of P2 (cf. Figure 4.I).
 319 However, both studies show a stabilization of the seabed elevation over the last 4 days
 320 of the 6-day period. Similar conclusions can be drawn regarding the length of the
 321 zone containing no sediment adjacent to the wave-maker (cf. Figure 4.G). An initial
 322 increase between 2 and 3 meters can be observed, with stability achieved in the later
 323 stages of the simulations. Finally, Figure 4.J shows the evolution of the shoreline
 324 position. Initially found at $x = 28.3\text{ m}$, all scenarios provoke a retreat of the shoreline:
 325 0.4 m in scenario 3, 0.3 m in scenario 4, and 2 m in scenario 5. The shorelines of the
 326 latter two converge, whereas scenario 3 shows an abrupt advance of the shoreline at
 327 day 5, with an attempt to return back to its stable state of $x = 30\text{ m}$. This tendency
 328 to evolve towards an equilibrium state indicates the presence of storm-like conditions;
 329 the seabed has been flattened, the sandbar has been destroyed and erosion can be
 330 observed at the coast (Grasso et al., 2011).

331 The comparisons made between the two 2-day simulations and the three 6-day
 332 simulations, in this given configuration, also reveal the little influence heritage has
 333 on the morphodynamic response. Both scenarios 1 and 2 have a comparable cumulative
 334 incoming wave energy density $E = \frac{1}{16} \int_0^T \rho g H_0^2 dt$ of 0.0591 J.m^{-2} . The resulting
 335 seabeds evolve towards similar profiles (reduction of the sandbar, increase of elevation
 336 of the plateau, and erosion at the coast), despite two very different forcing condi-
 337 tions. Similar conclusions can be drawn regarding the 6-day simulations, where the
 338 cumulative energy density of all three is equal to 0.177 J.m^{-2} .

339 5 Conclusion

340 Opti-Morph shows potential as a fast, robust, and low complexity morphody-
 341 namic model involving only two hyper-parameters. Despite using a basic hydrody-

342 namic model for the description of the complex coupling of hydrodynamic and mor-
 343 phodynamic processes, we can nevertheless observe that a numerical model based on
 344 an optimization theory works effectively, with comparable results to a state of the
 345 art hydro-morphodynamic model requiring the tuning of dozens of hyper-parameters.
 346 Long-term simulations also show typical morphodynamic behavior, with the tendency
 347 of the seabed to evolve towards an equilibrium state. These results demonstrate the
 348 tremendous potential of Opti-Morph, a constrained energy minimization morphody-
 349 namic model.

350 **Acknowledgments**

351 The experimental observations presented here were collected as part of the COPTER
 352 project (LEGI, France), with the help of Hervé Michallet and Adrien Lambert, and
 353 under the supervision of GLADYS (www.gladys-littoral.org). GLADYS also funded
 354 the project at the origin of the shore optimizer developed herein.

355 All data, models, and code generated or used during the study appear in the
 356 submitted article.

357 **Appendix A Mathematical Developments**

358 In this section, we detail some of the mathematical results needed in the imple-
 359 mentation of the Opti-Morph model, specifically the calculation of the gradient of the
 360 cost function J (Eq. (8)) with regard to the bathymetry ψ , which in turn requires the
 361 gradient of the wave height function (Eq. (7)) with regard to ψ . With the current
 362 choice of hydrodynamic model, this can be achieved analytically. With more sophis-
 363 ticated hydrodynamic models this is not always possible. In these cases, if the source
 364 code of the model is available, the calculation of the gradient can be performed using
 365 automatic differentiation of programs (Griewank & Walther, 2008; Hascoet & Pascual,
 366 2004) directly providing a computer program for the gradient.

367 **A1 Gradient of the Cost Function with respect to the Bathymetry**

Opti-Morph requires the evaluation of gradient of the functional J with re-
 spect to the bathymetry ψ , denoted $\nabla_{\psi}J$. For a general functional of the form
 $J(\psi(x), H(\psi(x)))$ involving dependencies with respect to the bathymetry and hydro-
 dynamic quantities H , this sensitivity can be expressed using the chain rule:

$$\nabla_{\psi}J = \nabla_{\psi}J + \nabla_H J \nabla_{\psi}H \tag{A1}$$

368 where $\nabla_{\psi}H$ requires the linearization of the hydrodynamic model, and ψ is a para-
 369 metric representation of the bathymetry.

In situations where this linearization is impossible, for instance because the hy-
 drodynamic model is a black-box, or too complex, the gradient can be obtained using
 first-order finite difference approximations:

$$\nabla_{\psi}J|_i \approx \frac{J(\psi(x + \varepsilon e_i), H(\psi(x + \varepsilon e_i))) - J(\psi(x), H(\psi(x)))}{\varepsilon} \tag{A2}$$

370 where $e_i(x_j) = \delta_{ij}$, the Kronecker delta. Typical relative value of ε is about three order
 371 of magnitude lower than the local water depth with a minimum value of 0.1 mm . A
 372 second-order approximation can be used as well as doubling the cost of the evaluation.
 373 For the sake of simplicity, we have omitted the time dependency in the formulas.

374 **A2 Gradient of the Wave Height with respect to the Bathymetry**

This section is devoted to the calculation of the gradient of the wave height H ,
 given by (7), with regards to the seabed elevation ψ and denoted $\nabla_{\psi}H$. Being as

$h = h_0 - \psi$, the derivation of the third line of (7) with regards to ψ is immediate. The calculation of the gradient of the first line of (7) is analogous to that of the second. It remains to differentiate the second line of (7) with regards to ψ . Observing that the chain rule yields for all $x, t \in \Omega_S \times [0, T]$ with $x \geq d_w$,

$$\nabla_\psi H(x, t) = H_0^w(x, t) \nabla_\psi K_S(x, t) + \nabla_\psi H_0^w(x, t) K_S(x, t), \quad (\text{A3})$$

and that the term $\nabla_\psi H_0^w(x, t)$ can be determined iteratively, using $\nabla_\psi H_0 = 0$, it remains to determine $\nabla_\psi K_S(x, t)$. Injecting the definitions of n , C and C_g , given in (4), yields

$$K_S = \left[\tanh(kh) \left(1 + \frac{2kh}{\sinh(kh)} \right) \right]^{1/2}. \quad (\text{A4})$$

For the sake of simplicity, let $U = \tanh(kh) \left(1 + \frac{2kh}{\sinh(kh)} \right)$ and $X = kh$. Equation (A4) becomes

$$\nabla_\psi K_S = -\frac{1}{2} U^{-3/2} \nabla_\psi U, \quad (\text{A5})$$

and we have

$$\nabla_\psi U = \nabla_\psi X \left[\frac{1}{\cosh^2(X)} \left(1 + \frac{2X}{\sinh(X)} \right) + 2 \tanh(X) \frac{\sinh(X) - X \cosh(X)}{\sinh^2(X)} \right], \quad (\text{A6})$$

with $\nabla_\psi X = h \nabla_\psi k + k \nabla_\psi h = h \nabla_\psi k - k$. Moreover, differentiating both sides of the dispersion equation (1) by ψ gives

$$k_\psi = \frac{k^2}{\cosh(kh) \sinh(kh) + kh}. \quad (\text{A7})$$

375 Combining (A5),(A6), and (A7), we obtain $\nabla_\psi K_S$, and therefore $\nabla_\psi H$.

376 References

- 377 Andrews, D. G., & McIntyre, M. E. (1978). An exact theory of nonlinear waves on
378 a lagrangian-mean flow. *Journal of Fluid Mechanics*, *89*(4), 609646. doi: 10
379 .1017/S0022112078002773
- 380 Beakawi Al-Hashemi, H. M., & Baghabra Al-Amoudi, O. S. (2018). A review on the
381 angle of repose of granular materials. *Powder Technology*, *330*, 397-417. doi:
382 https://doi.org/10.1016/j.powtec.2018.02.003
- 383 Bouchette, F. (2017, March). *Coastal defense strategy along hatzuk beach (north-*
384 *ern tel aviv, israel). insights from the copter physical experimentation with*
385 *moveable bed* (Tech. Rep. No. 17-1). Nîmes: BRL Ingénierie.
- 386 Bouharguane, A., Azerad, P., Bouchette, F., Marche, F., & Mohammadi, B. (2010,
387 06). Low complexity shape optimization and a posteriori high fidelity vali-
388 dation. *Discrete and Continuous Dynamical Systems-series B - DISCRETE*
389 *CONTIN DYN SYS-SER B*, *13*. doi: 10.3934/dcdsb.2010.13.759
- 390 Bouharguane, A., & Mohammadi, B. (2012, 03). Minimization principles
391 for the evolution of a soft sea bed interacting with a shallow. *Inter-*
392 *national Journal of Computational Fluid Dynamics*, *26*, 163-172. doi:
393 10.1080/10618562.2012.669831
- 394 Briand, M.-H., & Kamphuis, J. (1993, 07). Sediment transport in the surf zone: A
395 quasi 3-d numerical model. *Coastal Engineering*, *20*, 135-156. doi: 10.1016/
396 0378-3839(93)90058-G
- 397 Bugajny, N., Furmanczyk, K., Dudzinska-Nowak, J., & Papliska-Swerpel, B. (2013,
398 01). Modelling morphological changes of beach and dune induced by storm on
399 the southern baltic coast using xbeach (case study: Dziwnow spit). *Journal of*
400 *Coastal Research*, *1*, 672-677. doi: 10.2112/SI65-114.1

- 401 Coeffe, Y., & Pechon, P. (1982, 01). Modelling of sea-bed evolution under waves ac-
402 tion. *Proc. 18th ICCE*, 1. doi: 10.9753/icce.v18.71
- 403 Daly, C. (2009). Low frequency waves in the shoaling and nearshore zone a vali-
404 dation of xbeach. *Erasmus Mundus Master in Coastal and Marine Engineering*
405 *and Management (CoMEM)*, Delft University of Technology.
- 406 Dean, R., & Dalrymple, R. (2004, 03). Coastal processes with engineering applica-
407 tions. *Coastal Processes with Engineering Applications*, by Robert G. Dean and
408 Robert A. Dalrymple, pp. 487. ISBN 0521602750. Cambridge, UK: Cambridge
409 University Press, March 2004..
- 410 de Vriend, H., Bakker, W., & Bilsse, D. (1994, 07). A morphological behaviour model
411 for the outer delta of mixed-energy tidal inlets. *Coastal Engineering*, 23, 305-
412 327. doi: 10.1016/0378-3839(94)90008-6
- 413 Ding, Y., Wang, S., & Jia, Y. (2006, 11). Development and validation of
414 a quasi-three-dimensional coastal area morphological model. *Journal*
415 *of Waterway Port Coastal and Ocean Engineering*, 132, 462476. doi:
416 10.1061/(ASCE)0733-950X(2006)132:6(462)
- 417 Droenen, N., & Deigaard, R. (2007, 03). Quasi-three-dimensional modelling of the
418 morphology of longshore bars. *Coastal Engineering*, 54, 197215. doi: 10.1016/
419 j.coastaleng.2006.08.011
- 420 Fleming, C., & Hunt, J. (1977, 11). Application of sediment transport model. In
421 (p. 1184-1202). doi: 10.1061/9780872620834.070
- 422 Galappatti, G., & Vreugdenhil, C. (1985). A depth-integrated model for suspended
423 sediment transport. *Journal of Hydraulic Research*, 23(4), 359-377.
- 424 Grasso, F., Michallet, H., & Barthlemy, E. (2011). Experimental simulation of
425 shoreface nourishments under storm events: A morphological, hydrodynamic,
426 and sediment grain size analysis. *Coastal Engineering*, 58(2), 184-193. doi:
427 https://doi.org/10.1016/j.coastaleng.2010.09.007
- 428 Gravens, M. (1997, 08). An approach to modeling inlet and beach evolution. In
429 (p. 4477-4490). doi: 10.1061/9780784402429.348
- 430 Griewank, A., & Walther, A. (2008). *Evaluating derivatives: Principles and tech-*
431 *niques of algorithmic differentiation* (Second ed.). Society for Industrial and
432 Applied Mathematics. doi: 10.1137/1.9780898717761
- 433 Hascoet, L., & Pascual, V. (2004). Tapenade user's guide. In *Inria technical report*
434 (p. 1-31). INRIA.
- 435 Hasselmann, K., Barnett, T., Bouws, E., Carlson, H., Cartwright, D., Enke, K., ...
436 Walden, H. (1973, 01). *Measurements of wind-wave growth and swell decay*
437 *during the joint north sea wave project (jonswap)* (Tech. Rep.). Hamburg,
438 Germany: Deutsches Hydrographisches Institut.
- 439 Hattori, M., & Kawamata, R. (1980). Onshore-offshore transport and beach
440 profile change. In *Coastal engineering 1980* (p. 1175-1193). doi: 10.1061/
441 9780872622647.072
- 442 Holthuijsen, L., Booij, N., & Herbers, T. (1989, 05). a prediction model for station-
443 ary, short crested waves in shallow water with ambient current. *Coastal Engi-*
444 *neering*, 13, 23-54. doi: 10.1016/0378-3839(89)90031-8
- 445 Isèbe, D., Azerad, P., Bouchette, F., Ivorra, B., & Mohammadi, B. (2008). Shape
446 optimization of geotextile tubes for sandy beach protection. *International*
447 *Journal for Numerical Methods in Engineering*, 74(8), 1262-1277. doi:
448 10.1002/nme.2209
- 449 Isèbe, D., Azerad, P., Mohammadi, B., & Bouchette, F. (2008). Optimal shape de-
450 sign of defense structures for minimizing short wave impact. *Coastal Engineer-*
451 *ing*, 55(1), 35-46. doi: 10.1016/j.coastaleng.2007.06.006
- 452 Johnson, H., Brker, I., & Zyserman, J. (1995, 08). Identification of some relevant
453 processes in coastal morphological modelling. In (p. 2871-2885). doi: 10.1061/
454 9780784400890.208
- 455 Kana, T., Hayter, E., & Work, P. (1999, 03). Mesoscale sediment transport at south-

- 456 eastern u.s. tidal inlets: conceptual model applicable to mixed energy settings.
 457 *Journal of Coastal Research*, 15, 303-313.
- 458 Larson, M., & Kraus, N. (1989, 07). *Sbeach: Numerical model for simulating storm-*
 459 *induced beach change. report 1. empirical foundation and model development*
 460 (Tech. Rep.). Washington, DC, USA: DEPARTMENT OF THE ARMY US
 461 Army Corps of Engineers.
- 462 Larson, M., Kraus, N., & Byrnes, M. (1990, 05). *Sbeach: Numerical model for simu-*
 463 *lating storm-induced beach change. report 2. numerical formulation and model*
 464 *tests* (Tech. Rep.). Washington, DC, USA: DEPARTMENT OF THE ARMY
 465 US Army Corps of Engineers.
- 466 Latteux, B. (1980, 03). Harbour design including sedimentological problems using
 467 mainly numerical technics. In (p. 2213-2229). doi: 10.1061/9780872622647
 468 .133
- 469 Lesser, G., Roelvink, D. J., Kester, J., & Stelling, G. (2004, 10). Development and
 470 validation of a three-dimensional morphological model. *Coastal Engineering*,
 471 51, 883-915. doi: 10.1016/j.coastaleng.2004.07.014
- 472 Maruyama, K., & Takagi, T. (1988, 01). A simulation system of near-shore sediment
 473 transport for the coupling of the sea-bottom topography, waves and currents.
 474 *Proc. IAHR Symp. Math. Mod. Sed. Transp. Coastal Zone*, 300-309.
- 475 Mohammadi, B., & Bouchette, F. (2014, 01). Extreme scenarios for the evolution of
 476 a soft bed interacting with a fluid using the value at risk of the bed character-
 477 istics. *Computers and Fluids*, 89, 7887. doi: 10.1016/j.compfluid.2013.10.021
- 478 Mohammadi, B., & Bouharguane, A. (2011, 01). Optimal dynamics of soft shapes in
 479 shallow waters. *Computers and Fluids*, 40, 291-298. doi: 10.1016/j.compfluid
 480 .2010.09.031
- 481 Munk, W. (1949, 12). The solitary wave theory and its application to surf prob-
 482 lems. *Annals of the New York Academy of Sciences*, 51, 376 - 424. doi: 10
 483 .1111/j.1749-6632.1949.tb27281.x
- 484 Murray, A. B. (2007). Reducing model complexity for explanation and prediction.
 485 *Geomorphology*, 90(3), 178-191. (Reduced-Complexity Geomorphological Mod-
 486 elling for River and Catchment Management) doi: [https://doi.org/10.1016/j](https://doi.org/10.1016/j.geomorph.2006.10.020)
 487 [.geomorph.2006.10.020](https://doi.org/10.1016/j.geomorph.2006.10.020)
- 488 Nairn, R., & Southgate, H. (1993, 02). Deterministic profile modelling of nearshore
 489 processes. part 2. sediment transport and beach profile development. *Coastal*
 490 *Engineering*, 19, 57-96. doi: 10.1016/0378-3839(93)90019-5
- 491 Nicholson, J., Brker, I., Roelvink, D. J., Price, D., Tanguy, J.-M., & Moreno, L.
 492 (1997, 07). Intercomparison of coastal area morphodynamic models. *Coastal*
 493 *Engineering - COAST ENG*, 31, 97-123. doi: 10.1016/S0378-3839(96)00054-3
- 494 of Engineers, U. A. C. (2002). *Coastal engineering manual, engineer manual 1110-2-*
 495 *1100*. Washington, D.C.: Author.
- 496 Quick, M. (1991). Onshore-offshore sediment transport on beaches. *Coastal Engi-*
 497 *neering*, 15, 313-332.
- 498 Reineck, H.-E., & Singh, I. B. (1973). *Depositional sedimentary environments;*
 499 *with reference to terrigenous clastics [by] h.-e. reineck [and] i. b. singh* [Book].
 500 Springer-Verlag Berlin, New York.
- 501 Roelvink, D. J. (1993, 02). Dissipation in random wave groups incident on a beach.
 502 *Coastal Engineering - COAST ENG*, 19, 127-150. doi: 10.1016/0378-3839(93)
 503 90021-Y
- 504 Roelvink, D. J., Reniers, A., van Dongeren, A., Thiel de Vries, J., Lescinski, J., &
 505 McCall, R. (2010, 01). *Xbeach model description and manual* (Tech. Rep.).
 506 Delft, Netherlands: Unesco-IHE Institute for Water Education, Deltares and
 507 Delft University of Technology.
- 508 Roelvink, D. J., Reniers, A., van Dongeren, A., Thiel de Vries, J., McCall, R.,
 509 & Lescinski, J. (2009, 11). Modelling storm impacts on beaches, dunes
 510 and barrier islands. *Coastal Engineering*, 56, 1133-1152. doi: 10.1016/

- 511 j.coastaleng.2009.08.006
- 512 Roelvink, D. J., Walstra, D.-J., & Chen, Z. (1995, 08). Morphological modelling of
513 keta lagoon case. In (p. 3223-3236). doi: 10.1061/9780784400890.233
- 514 Roelvink, J. A., Van Banning, G. K. F. M., & Verwey, A. (1994). Design and
515 development of delft3d and application to coastal morphodynamics, 1st inter-
516 national conference, hydroinformatics 94. In *Hydroinformatics 94, hydroinforma-*
517 *matics -proceedings-, 1st international conference, hydroinformatics 94* (Vol. 1,
518 p. 451-456). Rotterdam: Balkema.
- 519 Ruessink, G., & Terwindt, J. (2000, 02). The behaviour of nearshore bars on the
520 time scale of years: A conceptual model. *Marine Geology, 163*, 289-302. doi:
521 10.1016/S0025-3227(99)00094-8
- 522 Soulsby, R. (1987, 11). Calculating bottom orbital velocity beneath waves. *Coastal*
523 *Engineering - COAST ENG, 11*, 371-380. doi: 10.1016/0378-3839(87)90034-2
- 524 Soulsby, R. (1997). *Dynamics of marine sands*. Thomas Telford Publishing. doi: 10
525 .1680/doms.25844
- 526 Walstra, D.-J., Roelvink, D. J., & Groeneweg, J. (2000, 01). Calculation
527 of wave-driven currents in a 3d mean flow model. In (Vol. 276). doi:
528 10.1061/40549(276)81
- 529 Wang, H., Miao, G., & Lin, L.-H. (1993, 06). A timedependent nearshore morpho-
530 logical response model. In (p. 2513-2527). doi: 10.1061/9780872629332.192
- 531 Watanabe, A., Maruyama, K., Shimizu, T., & Sakakiyama, T. (1986, 12). Nu-
532 merical prediction model of three-dimensional beach deformation around
533 a structure. *Coastal Engineering Journal, 29*, 179-194. doi: 10.1080/
534 05785634.1986.11924437
- 535 Williams, J., Esteves, L., & Rochford, L. (2015, 05). Modelling storm responses on a
536 high-energy coastline with xbeach. *Modeling Earth Systems and Environment,*
537 *1*. doi: 10.1007/s40808-015-0003-8
- 538 Yamaguchi, M., & Nishioka, Y. (1985, 11). Numerical simulation on the change
539 of bottom topography by the presence of coastal structures. In (p. 1732-1748).
540 doi: 10.1061/9780872624382.118
- 541 Zimmermann, N., Trouw, K., Wang, L., Mathys, M., Delgado, R., & Verwaest, T.
542 (2012, 12). Longshore transport and sedimentation in a navigation chan-
543 nel at blankenberge (belgium). *Coastal Engineering Proceedings, 1*. doi:
544 10.9753/icce.v33.sediment.111
- 545 Zyserman, J., & Johnson, H. (2002, 05). Modelling morphological processes in the
546 vicinity of shore-parallel breakwaters. *Coastal Engineering, 45*, 261284. doi: 10
547 .1016/S0378-3839(02)00037-6